Supporting Information

High-Affinity Detection and Capture of Heavy Metal Contaminants using Block Polymer Composite Membranes

Yizhou Zhang,[†] Joseph R. Vallin,[†] Jugal K. Sahoo,[†] Feng Gao,[†] Bryan W. Boudouris,[‡,§] Matthew J. Webber,[†] and William A. Phillip[†,*]

[†]Department of Chemical and Biomolecular Engineering, University of Notre Dame, Notre Dame, Indiana 46556, United States

[‡]Charles D. Davidson School of Chemical Engineering and [§]Department of Chemistry, Purdue University, West Lafayette, Indiana 47907, United States

* To whom correspondence should be addressed: wphillip@nd.edu

Detailed Experimental Procedure and Calculations

No unexpected or unusually high safety hazards were encountered. Respiratory and skin exposure to heavy metal salts and associated solutions should be avoided.

1. Fabrication of functional macroporous polysulfone membrane.

All chemicals were purchased from Sigma-Aldrich and used as received unless otherwise noted. The membrane casting solution was prepared by sequentially dissolving 8.0% (by weight) polysulfone ($M_n \sim 22$ kg mol^{-1}) and 2.0% (by weight) polystyrene-*b*-poly(acrylic acid) (PS-PAA) diblock copolymer in the 2-pyrrolidone (i.e., 10% total polymer content by weight in the final casting solution). The PS-PAA (Polymer Source, Inc.) has a number averaged molecular weight of $M_n = 84$ kg mol^{-1}, a dispersity of 1.1, and weight fraction values of $w_{PS} = 0.84$ and $w_{PAA} = 0.16$, respectively. The solution was stirred at 40 °C until a homogeneous solution was obtained, followed by let it sit without stirring at room temperature for ~8 h, to allow the solution to degas.

Membranes were fabricated using the surface-segregation and vapor-induced phase separation (SVIPS) methodology in a humidified environment. A controlled humidity chamber with the relative humidity carefully regulated from 94% to 99% and the temperature monitored

between 24 °C and 27 °C was used for membrane casting. To cast a membrane, a pre-determined amount of polymer casting solution was pipetted on top a glass substrate (Corning), and the solution was immediately drawn into a uniform thin-film via a doctor blade (Mitutoyo) set with a gate height of 305 μm. The thin film was exposed to the humid air for a predetermined amount of time prior to the opaque thin-film being immersed in the non-solvent (DI water, R = 18 M Ω) bath. Subsequently, the membrane was annealed in a bath of DI water heated to 80 °C for 24 h in order to bring the poly(acrylic acid) brushes to the pore wall of the macroporous polysulfone matrix. The heat source was turned off, and the DI water bath was allowed to cool to room temperature. The membranes were then hand punched into 2.5-cm circular sections, and they were stored in the DI water bath until further functionalization, adsorption, or transport experiments were conducted.

2. Synthesis of 6-(2, 2': 6', 2''-terpyridin-4'-yloxy) hexanoic acid.

The synthesis of 6-(2, 2': 6', 2''-terpyridin-4'-yloxy) hexanoic acid (TerP) was performed following a procedure reported previously in the literature.[1] Typically, powdered KOH (1.85 g, excess) was added to DMSO (10-12 mL) at 65 °C to form a suspension. Ɛ-Caprolactone (1.49 g, 13.07 mM) was added dropwise to the stirred solution. After 30 minutes, 4'-chloro-2, 2':6', 2''-terpyridine (1.74 g, 6.49 mM) was added. The mixture was stirred for 48 h at 65 °C. After 48 h, 400 mL of DI water was added to the reaction mixture. Concentrated HCl (1 M) was then added dropwise to the transparent solution until precipitation of a white solid was observed (pH ~ 6). The aqueous phase was filtered using a Buchner funnel and the crude product was recrystallized in tetrahydrofuran (THF) and dried *in vacuo* to obtain the desired product. ^{1}H nuclear magnetic resonance (^{1}H-NMR) spectra of the TerP was acquired on a Bruker AVANCE III HD 400 spectrometer with deuterated dimethyl sulfoxide (DMSO-d_6) as the solvent. Mass spectrometry data was obtained using an HPLC-MS in-line system, which houses an Advion BioSciences

Expression compact mass spectrometer (CMS-L) unit with electrospray negative ionization (ESI) source. The samples were measured in methanol (0.1 mg mL^{-1}).

3. Membrane functionalization via carbodiimide coupling reactions.

The pore wall chemistry of the PAA-functionalized polysulfone membranes was further modified *via* solid-state coupling reactions following previously-reported protocols using 1-ethyl-3-(3-dimethylaminopropyl) carbodiimide hydrochloride (EDC·HCl) as the carboxyl activating agent.[2, 3] Through the use of this simple reaction methodology, branched polyethylenimine (PEI) and 6-([2,2':6',2''-terpyridin]-4'-yloxy) hexanoic acid (terpyridine, TerP) were sequentially attached onto the pore wall. The carbodiimide coupling reaction that converted the pore wall chemistry from poly(acrylic acid) to branched polyethylenimine was carried out by immersing pieces of a poly(acrylic acid) functionalized polysulfone membrane into an aqueous solution containing 5 mM polyethylenimine (M_n ~ 60 kg mol^{-1}), 50 mM EDC·HCl (Chem-Impex International, Inc.), 250 mM hydroxybenzotriazole (HOBt), and 100 mM $NaHCO_3$. The 60 kg mol^{-1} branched polyethylenimine was selected for the functionalization process because its hydrated size is much smaller than the pore size of the Psf-PAA membrane. The solution pH was monitored by using an Accumet AP115 portable pH meter (Fisher scientific, Waltham, MA), and the pH was adjusted by diluting hydrochloric acid (HCl) in the solution until a neutral pH was achieved. The mixture was then covered and left to react at room temperature for 4 days, followed by removing the membrane from solution and rinsing it thoroughly with DI water. In this manner, the PEI functionalized membrane was ready for the further covalent attachment of the terpyridine chemistry. The conversion of branched PEI lined pore wall chemistry into terpyridine follows a similar carbodiimide coupling reaction protocol using the EDC·HCl as the carboxyl activating agent. Specifically, PEI functionalized membranes were submerged in an ethanol solution

containing 25 mM terpyridine, 10 mM EDC·HCl and 25 mM HOBt in a 150 mL pressure vessel (Chemglass). The solution was heated to 70 °C for 12 h followed by cooling the solution to room temperature, prior to removing the membrane from the vessel and rinsing thoroughly with DI water. Both the branched PEI and terpyridine functionalized membranes were stored in DI water baths before they were further utilized in the static cation adsorption and transport experiments.

4. Nanostructural and chemical characterization.

A Magellan 400 (FEI) Digital Field Emission Scanning Electron Microscope (FE-SEM) was utilized to characterize the nanoscale morphology of the various membranes. For membrane surface characterization, samples of vacuum-dried membranes were cut into 5.0 mm × 5.0 mm pieces from larger sheets using a razor blade. Samples for cross-sectional imaging analysis were prepared by fracturing after submerging the membranes in a bath of liquid nitrogen for ~ 30 s. Subsequently, sample pieces were mounted on standard aluminum SEM pin stubs (Ted Pella, Inc.) using conductive carbon tape and were sputter-coated with ~1.5 nm of iridium prior to loading the samples into the microscope. Micrographs were captured at a working distance of 4.0 mm, with accelerating voltages ranging from 5 to 10 kV and beam current ranging from 6.3 to 13 pA.

The chemical compositions of the membranes were analyzed by using a Jasco Fourier Transform Infrared (FT/IR-6300) spectrometer equipped with an interchangeable attenuated total reflectance (ATR) crystal plate. Prior to analysis, pieces of membrane samples were vacuumed-dried and stored in a clean scintillation vial. The ATR-FT/IR spectra was collected over a range of $650.0 \leq \nu \leq 4{,}000$ cm^{-1}. The surface elemental analysis was performed by using a PHI VersaProbe II X-Ray Photoelectron Spectrometer (XPS). Membrane samples were mounted on a stub by using double sided tape and were loaded into the XPS chamber under ultra-high vacuum (1×10^{-8} torr) for photoelectron spectrum collection. The binding energy of the C 1s shell of amorphous carbon

(284.5 eV) was utilized as a reference during the measurement of each sample to account for charging The surface elemental compositions were determined through the use of a numerical integration routine in the Phi Multipak software package. The nitrogen (N) to oxygen (O) ratio was then calculated based on the elemental composition corresponding to each membrane sample.

5. Cation adsorption experiments for heavy metal binding assessment.

The static equilibrium cation adsorption experiments of functionalized polysulfone membranes were performed based on membranes that were hand-punched into 2.5-cm circular sections. The cation binding isotherms were assessed using cupric chloride ($CuCl_2$) as a model solute. For PAA- and PEI-functionalized membranes, pieces of membranes were immersed in aqueous sodium hydroxide solutions (pH = 13) for ~ 8 h and rinsed with excess DI water for ~ 15 minutes prior to cation binding experiments. In this manner, the deprotonated carboxylic acid and ethylenimine chemistries were ready for subsequent cation adsorption experiment. The membranes were then submerged in excess amount of $CuCl_2$ solution (i.e., by immersing a piece of membrane that weight ~ 0.01 g in a bath of $CuCl_2$ solution at < 0.20 g of membrane per liter of cupric chloride solution) at concentrations between 1 and 150 mM (64 to 9.5×10^3 ppm) for ~ 8 h, and were subsequently rinsed with excess DI water for ~ 15 minutes to remove free and loosely bound copper ions remaining within the membrane structure. To completely release bound cations, copper containing membranes were relocated into separate scintillation vials containing 5 ml diluted hydrochloric acid (pH = 1) for ~ 8 h. The dilute hydrochloric acid solutions containing copper ions were stored to be analyzed by a Cary 60 ultraviolet-visible (UV-Vis) spectrophotometer that calculates the concentration of copper ions samples using Beer's Law, with the maximum in the absorbance for the copper (II) at λ = 830 nm.

To characterize the binding isotherm of the terpyridine functionalized membranes, samples were immersed in $CuCl_2$ solutions at concentrations between 0.1 and 1.0 mM (6.3 to 63 ppm) for ~8 h, with a packing ratio of 0.25 g membrane L^{-1}. Following the copper binding experiment, membranes were rinsed with DI water thoroughly for ~ 15 minutes to remove free and loosely bound copper, and then were transferred into individual scintillation vials containing 10 mL of a 50 mM ethylenediaminetetraacetic acid (EDTA) solution for ~ 8 h. The copper releasing experiments for Cu^{2+} bounded terpyridine-functionalized membranes were performed based on a packing ratio of 1.3 g membrane per liter of EDTA solution. The copper ion sequestered EDTA solution and the retentate solutions were analyzed via a Perkin Elmer Optima 8000 Inductively Coupled Plasma Optically Emitting Spectra (ICP-OES) to quantify the equilibrium cation concentration. Membranes were repeatedly regenerated and reused to collect adsorption experimental data.

The adsorption kinetics of the terpyridine-functionalized polysulfone membranes were assessed using a similar approach as followed in the isotherm study. To start with, pieces of 2.5-cm diameter circular sample disks were immersed into excess $CuCl_2$ solution (i.e., with a packing ratio > 0.1 g membrane L^{-1}) at a concentration of 10 mM. The membranes were submerged in the solution for a pre-determined amount of time ranging from 20 to 600 s. The membranes were rinsed with DI water before being transferred into individual scintillation vials containing 10 mL of a 50 mM EDTA solution. The membranes were left in the EDTA solution for ~ 8 h. After removing the membrane, and the copper concentration in the retentate solutions were analyzed using ICP-OES.

The adsorption experiments that analyzed static metal ion binding in the presence of multiple background electrolytes and the additional single solute metal ion adsorption experiments

were performed in a similar manner as the binding-isotherm experiments detailed above. In the experiments examining the effects of multiple background electrolytes adsorption experiment, 6 and 18 ppm Pb^{2+} and Cd^{2+} stock solutions were prepared by dissolving $Pb(NO_3)_2$ and $CdCl_2$ in DI water (R = 18 M Ω), artificial ground water (composed by 0.40 mM Mg^{2+}, 1.3 mM Ca^{2+}, 17 mM Na^+, 0.25 mM K^+, 0.52 mM SO_4^{2-}, 1.7 mM CO_3^{2-} and 5.7 mM Cl^-) and artificial sea water (composed by 54.5 mM Mg^{2+},10.5 mM Ca^{2+}, 480 mM Na^+, 10.2 mM K^+, 30.0 mM SO_4^{2-}, 2.36mM HCO_3^- and 561 mM Cl^-), respectively.[4, 5] In the single solute adsorption experiment, metal ion solutions were prepared by dissolving 18 ppm cation within DI water. A total number of 8 cations Co^{2+} ($CoCl_2$), Fe^{2+} ($FeCl_2$), Hg^{2+} ($HgCl_2$), Ni^{2+} ($NiCl_2$), Pd^{2+} ($PdCl_2$), Nd^{3+} ($Nd(NO_3)_3$), Sm^{3+} ($Sm(NO_3)_3$) and Zn^{2+} ($ZnCl_2$) were screened in addition to Cd^{2+}, Pb^{2+} and Cu^{2+}. $PdCl_2$ was dissolved in dilute acid with solution pH monitored at pH = 1 to enhance Pd^{2+} solubility. To start, PAA-functionalized, PEI-functionalized, and terpyridine-functionalized membranes were immersed in cation stock solutions based on a packing ratio of 2.0 g membrane L^{-1} for ~ 8 h. After removing the membrane samples, the retentate solutions were analyzed by ICP-OES to determine the residual cation concentrations. Heavy metal bonded membranes were repeatedly regenerated by using 50 mL diluted hydrochloric acid or EDTA solution for further cation binding experiments, expect PEI and TerP-lined membranes bound with Co^{2+} did not show release despite the presence of external stimuli.

6. Hydraulic permeability characterization and dynamic metal ion breakthrough experiments.

The 2.5 cm polysulfone membrane disks were assembled into a 10 ml stirred cell (EMD Millipore Amicon 8010) with surface layer facing the feed solution atop of a 2.5 cm PP/PE nonwoven support. Because the membranes have high hydraulic permeability that depleted the 10

ml stirred cell within seconds even at lower trans-membrane pressures (i.e., < 0.2 bar), the stirred cell was connected to an 800 mL stirred reservoir (EMD Millipore, Amicon 6028) to increase the capacity of feeding reservoir for continuous flow-through experiments. The stirred cell system was filled with DI water (R = 18 M Ω) with pH ~5.5 during hydraulic permeability assessment experiments. During the pH-responsive permeability experiment of PAA-functionalized polysulfone membranes, pH-adjusted solutions were prepared by diluting hydrochloric acid or dissolving sodium hydroxide in the DI water to prepared acidic (pH = 1) or basic (pH = 13) solutions, respectively. Solution pH was carefully monitored using an AP115 portable pH meter. A carefully regulated trans-membrane pressure ranging from 0.010 to 0.12 bar was applied using compressed nitrogen gas. The permeate solution was collected in a capped glass container that rested on an electronic balance, and the mass of permeate was recorded electronically every 3 s for up to 5 min to acquire a stable and accurate measurements of the flux through the membranes. Subsequently, the hydraulic permeabilities were determined using linear regressions based on the water flux acquired from multiple trans-membrane pressures.

The heavy metal breakthrough experiments were executed using a test bed comprised of three membranes stacked inside a stirred cell device. The test bed was prepared by stacking a Psf-PEI membrane on top of two Psf-TerP membranes. Due to the lower hydraulic permeability of the Psf-PEI membrane, this configuration provided better control over the rate of the pressure-mediated flow. A trans-membrane pressure ranging from ~0.2 to 0.3 bar was applied using compressed nitrogen gas to generate a permeate flux of ~200 L m^{-2} h^{-1}. $CdCl_2$, $PbCl_2$, $HgCl_2$, and $CuCl_2$ salts were used to prepare the mixed ion feed solutions. All feed solutions were formulated to contain the individual metal ions (Cd^{2+}, Pb^{2+}, Hg^{2+}, and Cu^{2+}) dissolved in DI water (R = 18 M Ω) at a concentration of 1 ppm. One feed solution contained 1 ppm each of Cd^{2+}, Pb^{2+}, and Hg^{2+}

and the other feed solution contained Cd^{2+} and Cu^{2+} at 1 ppm. The ion concentrations within the permeate solutions, which were collected at ~5 mL intervals, were analyzed by ICP-OES.

7. Fluorescence quenching experiments.

TerP-modified membranes were cut into pieces of 2.0 mm × 2.0 mm from larger sheets using a razor blade and were exposed to Cu^{2+} at different rententate solution concentrations. Membranes were rinsed thoroughly with DI water and transferred to a 24-well plate using forceps. Fluorescent images were captured using an EVOS-Auto-FL microscope with illumination from a DAPI (blue fluorescence) light cube and corresponding emission filters. All acquisition parameters were maintained constant across images. The resulting gray-scale images were processed by background subtraction using ImageJ and false-colored blue to reflect the wavelength of emitted light.[6] Fluorescence emission spectra from these same samples as were imaged was then collected between 386 to 600 nm using a multi-modal plate reader (Infinite M200 Pro, Tecan) with an excitation wavelength of 358 nm.

8. Calculation for hydraulic permeability of functionalized Psf membranes.

The pH-responsive hydraulic permeability of the Psf-PAA membranes is consistent with scaling analysis in the low Reynolds number limit. In this limit, the hydraulic permeability depends on the effective pore diameter to the fourth power, d_p^4. Analysis of the SEM micrographs of the membrane reveal a pore diameter on the order of ~500 nm. As depicted schematically in Figure S3, the extension of the PAA brushes on the pore walls constricts the pore diameter to a smaller value. There are N_{PAA} ~180 repeat units in a PAA brush with a molecular weight of 13 kg mol^{-1}. This corresponds to a brush length of ~38 nm assuming a charged polymer brush extend as rigid rod within good solvent[7-9]

$$L_{PAA} = N^{0.8} b = 38.2 \text{ nm} \quad \text{(S1)}$$

where b is the statistical segment length of PAA (~0.6 nm). In this instance, the permeability should be reduced by a factor of $(423.5/500)^4 = 0.51$ at high pH values when the PAA brushes extend. Given the approximate nature of this estimate, this is consistent with the ratio of the permeabilities observed experimentally at a value of 0.56.

In addition to impacting the metal capture characteristics of the membranes, the repeat unit chemistry directly impacts the configuration of the polymer brushes on the pore walls, and hence, the hydraulic permeabilities values of the membranes. These variations in permeability with the varied pore chemistries are demonstrated in Figure S15. The permeability values were calculated from the water fluxes measured as a function of applied pressure (Figure S2). The incorporation of branched PEI, which possesses a large hydrodynamic diameter, constricts the pore size and reduces the porosity relative to the Psf-PAA membrane, and both of these factors contribute to a more than one order of magnitude decline in hydraulic permeability. Compared to the Psf-PAA membranes that had a permeability of 2.5×10^4 L m^{-2} h^{-1} bar^{-1}, the Psf-PEI membranes had a permeability of 1.8×10^3 L m^{-2} h^{-1} bar^{-1}. However, the attachment of the more hydrophobic TerP moieties, which hinders the extension of the polymer brushes, increased the effective pore size and thus a large hydraulic permeability value of ~2.8×10^4 L m^{-2} h^{-1} bar^{-1}, similar to that of the original PAA-lined template, was recovered. In this manner, a high-performance adsorption membrane is prepared, with high cation binding capacity and affinity and an extremely high hydraulic permeability.

Supporting Figures

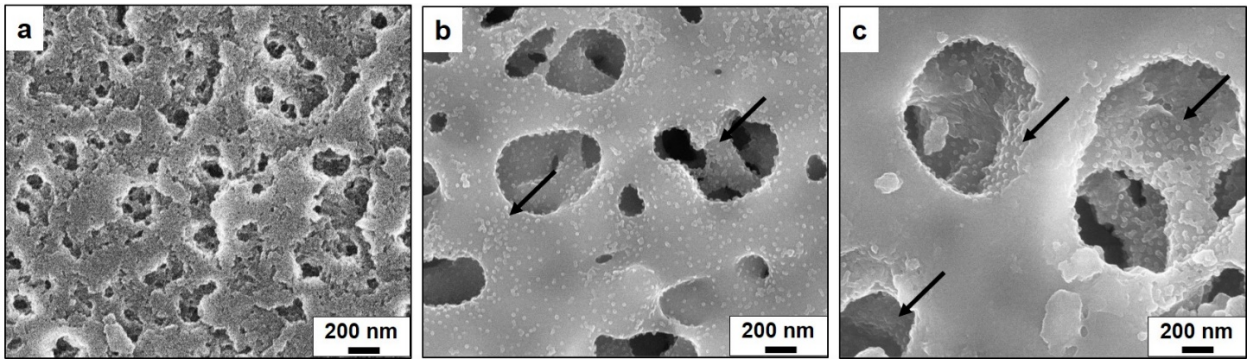

Figure S1. High-magnification SEM micrographs of the PSf-PAA membrane surface prepared from (a) 0 s, (b) 45 s, and (c) 90 s of vapor exposure. The surface morphology of the membrane produced without vapor exposure, as shown in (a), was guided by the non-solvent induced phase separation. Heterogeneous beads, which are labeled by black arrows in the image (b) and (c), were dispersed across the pore wall surfaces suggesting they are a result of the PAA that segregated to the pore wall of Psf matrix during vapor induced phase separation.

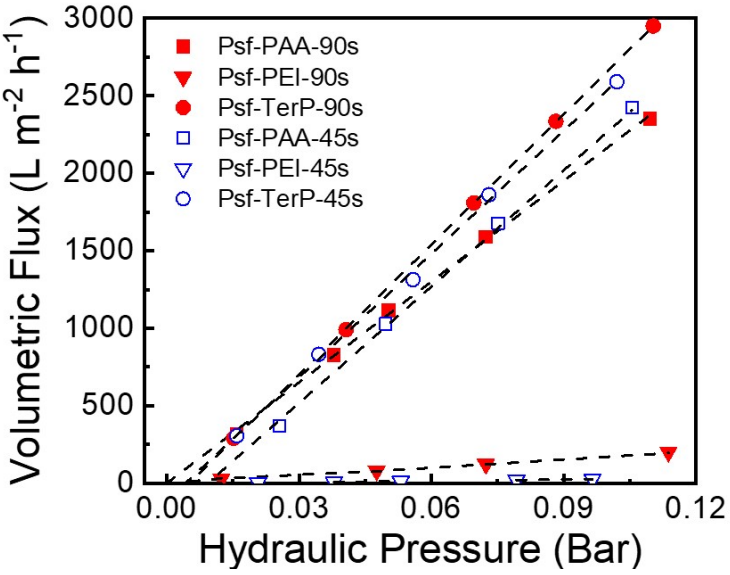

Figure S2. Volumetric flow rate versus applied pressure for functional Psf membranes that were generated from parent membranes fabricated with different vapor exposure periods. The hydraulic permeabilities were determined from the slope derived from the linear regression (dashed line), measured in DI water with a solution pH of 5.5.

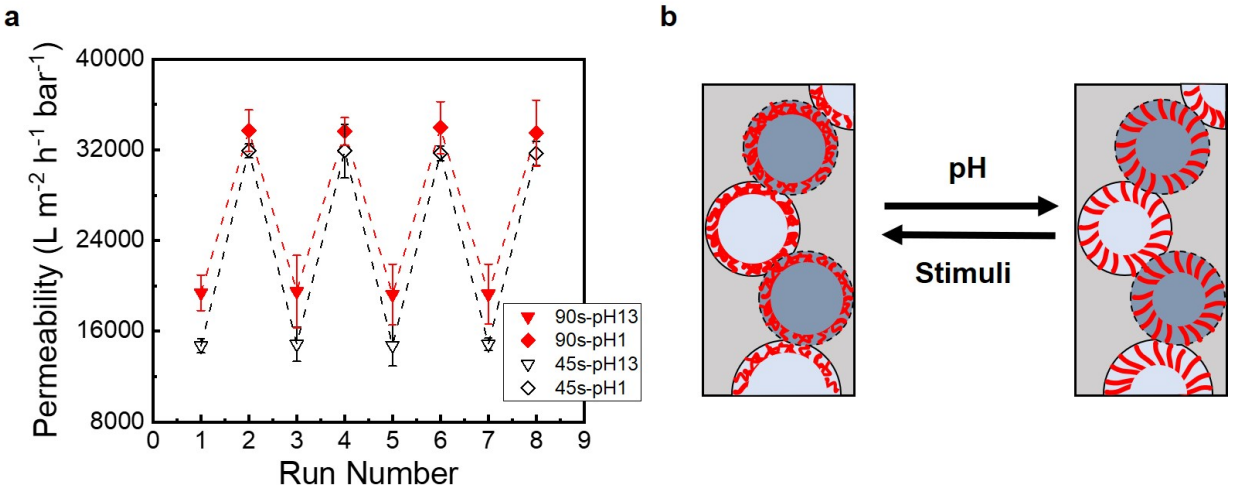

Figure S3. (a) The hydraulic permeabilities of Psf-PAA-45s and Psf-PAA-90s membranes as a function of solution pH. The permeability of the membrane was measured as it was exposed to solutions that alternated between pH=1 and pH=13. (b) The reversible and repeatable and change in permeability is a direct result of the extension and contraction of the PAA brushes that line the pore walls.

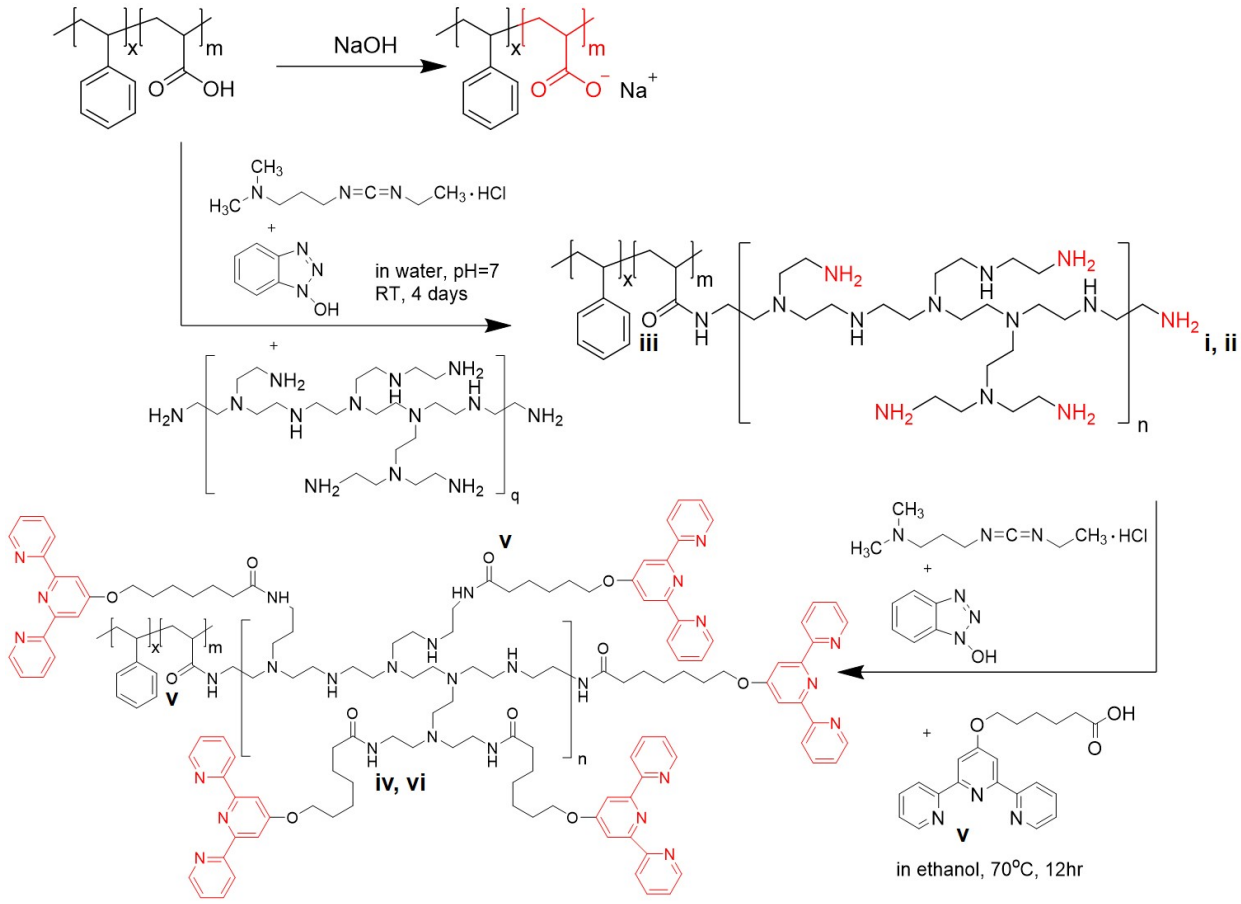

Figure S4. The full coupling reaction scheme utilized to the convert the pore wall chemistry from (i) PAA brushes to (ii) a PEI intermediate and finally (iii) the TerP-functionalized brushes. The chemical bonds labeled by the Roman numerals are associated with characteristic peaks that are highlighted in Figure S5.

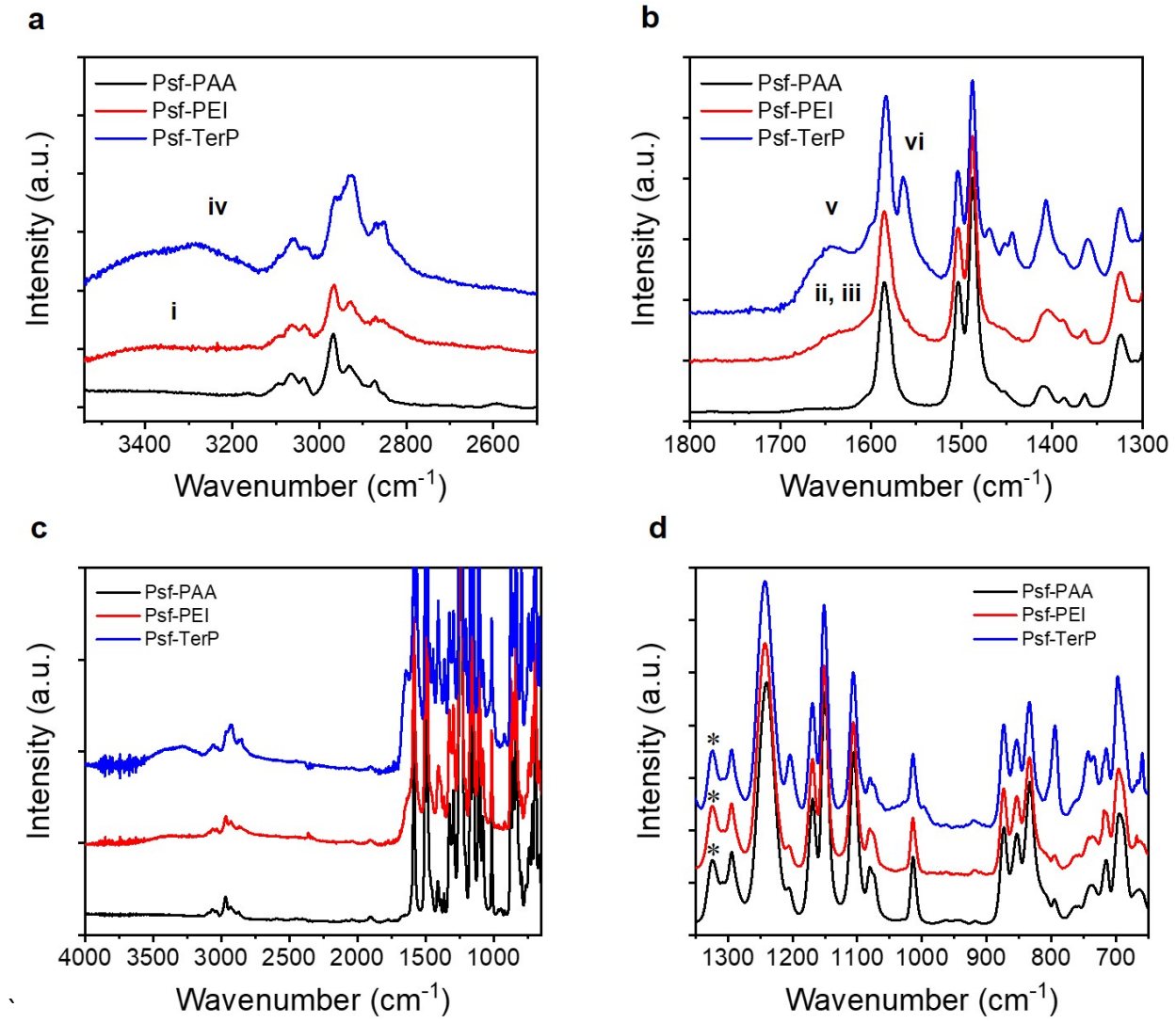

Figure S5. (a-b) FTIR monitors the successful conversion of the pore wall lining chemistry. The appearance of the peaks at ~3400 cm^{-1} (labeled as i) and ~1640 cm^{-1} (labeled as ii and iii) are consistent with the formation of an amide bond in the PEI functionalized membrane. The broad peak at ~ 3300 cm^{-1} (labeled as iv), ~ 1640 cm^{-1} (labeled as v) and ~1560 cm^{-1} (labeled as vi) suggests the formation of additional amide bond. The broad peak at ~ 1640 cm^{-1} (labeled as v) also suggests the addition of imines from the terpyridine molecule. (c) Full FTIR spectra of functionalized membranes scanned over a range of $650.0 \leq \nu \leq 4{,}000$ cm^{-1}. (d) Magnified FTIR spectra over a range of $650.0 \leq \nu \leq 1{,}350$ cm^{-1}. The peak intensities of the spectra were normalized using the characteristic sulfone adsorption at 1325 cm^{-1} (*).

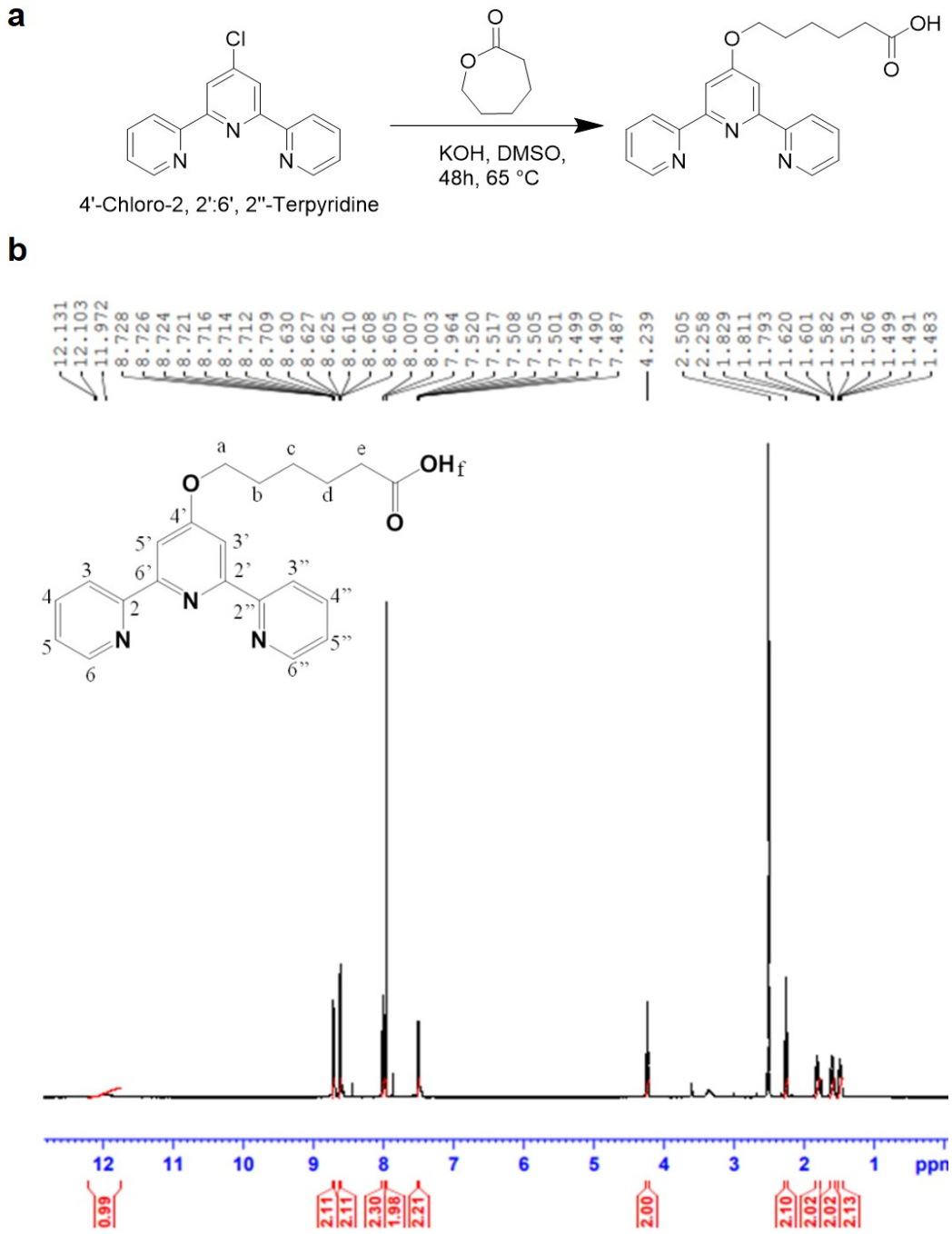

Figure S6. (a) The reaction scheme for synthesis of the 6-(2, 2′: 6′, 2′′-terpyridin-4′-yloxy) hexanoic acid (TerP). (b) ^{1}H NMR spectra of the TerP with DMSO-d_6 as the solvent. ^{1}H NMR [400 MHz, DMSO-d$_6$]: δ= 1.51, (*m*, 2H, Hc), 1.60 (*m*, 2H, H$_d$), 1.79 (*m*, 2H, H$_b$), 2.25 (*t*, J=7.2 Hz, 2H, H$_e$), 4.23 (*t*, J= 6.4 Hz, 2H, H$_a$), 7.5 (*ddd*, J=7.5, 4.8, 1.2, 2H, H$_{5,5''}$), 7.96 (*s*, 2H, H$_{3',5'}$), 8.00 (*td*, J= 7.6, 1.8, 2H, H$_{4,4''}$), 8.62 (*ddd*, J= 7.9, 2, 1, 2H, H$_{3,3''}$), 8.71 (*ddd*, J= 4.7, 1.7, 0.9, 2H, H$_{6,6''}$), 12.1 (*s*, 1H, H$_f$)

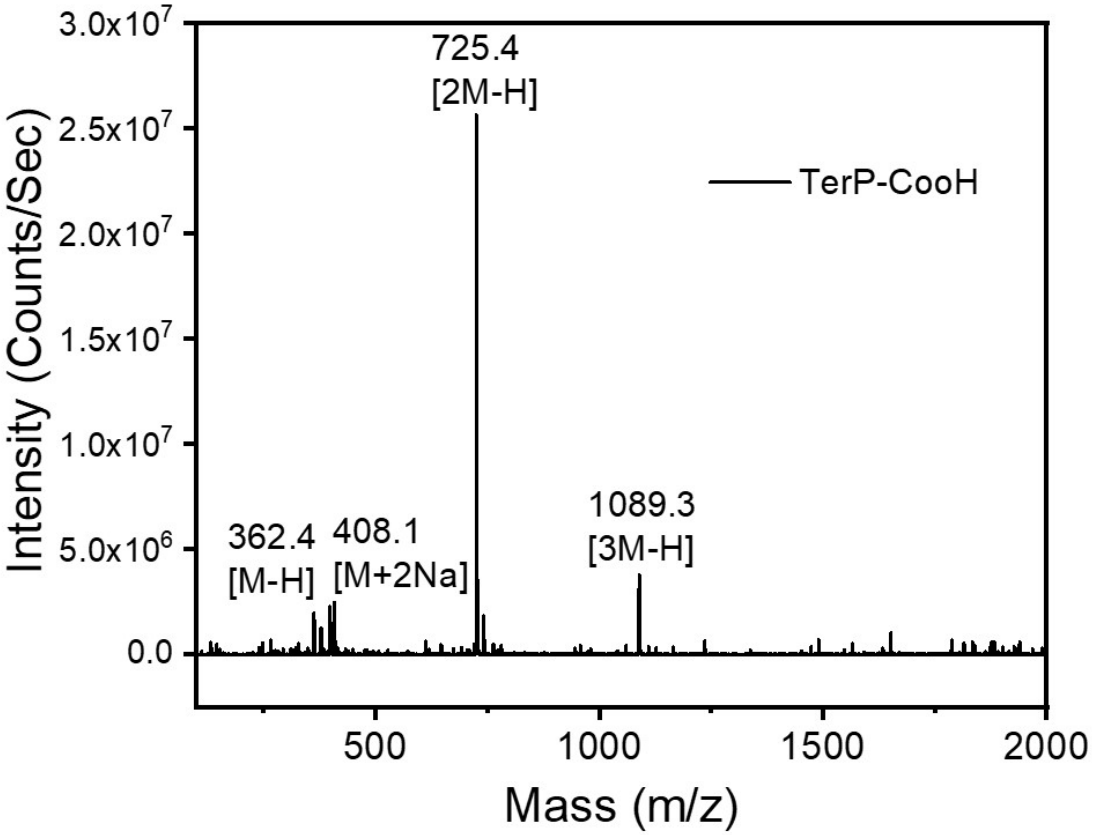

Figure S7. Mass spectrometric data of the 6-(2, 2′: 6′, 2′′-terpyridin-4′-yloxy) hexanoic acid: MS (ESI Negative) calculated for [M-H]- 362.42 g mol^{-1}, found: 362.4 g mol^{-1}. The peak at 725.4 g mol^{-1} is associated with dimers of the 6-(2, 2′: 6′, 2′′-terpyridin-4′-yloxy) hexanoic acid.

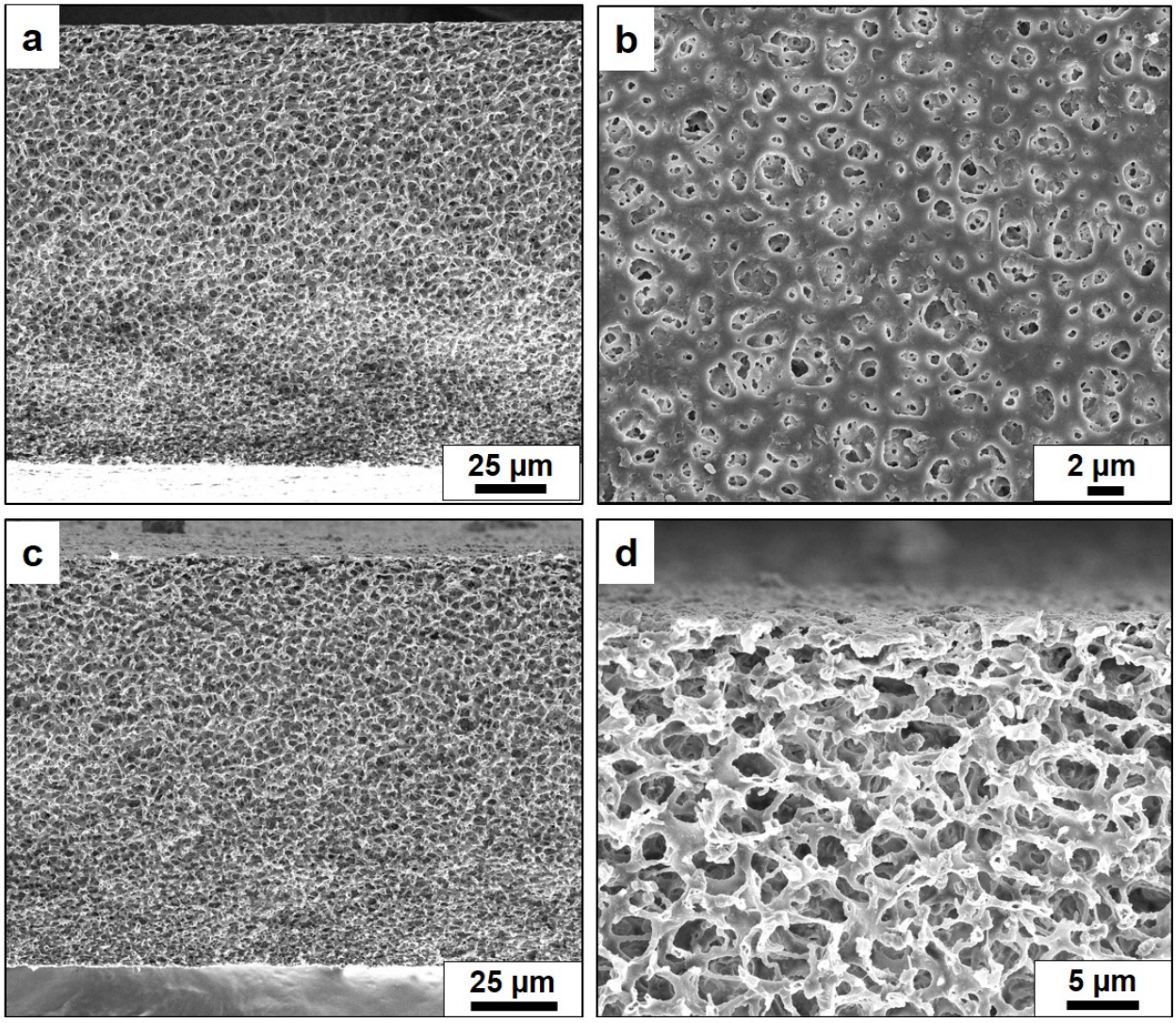

Figure S8. (a) A cross-sectional SEM micrograph of the Psf-PEI suggest the interconnected porous structure of the parent Psf-PAA membrane was retained. (b) PSf-TerP membrane surface, which suggests the changes in pore wall chemistry did not significantly alter the membrane morphology. (c-d) Cross-sectional SEM micrographs of the Psf-TerP membrane reveals the similar interconnected porous structure from the Psf-PAA membrane.

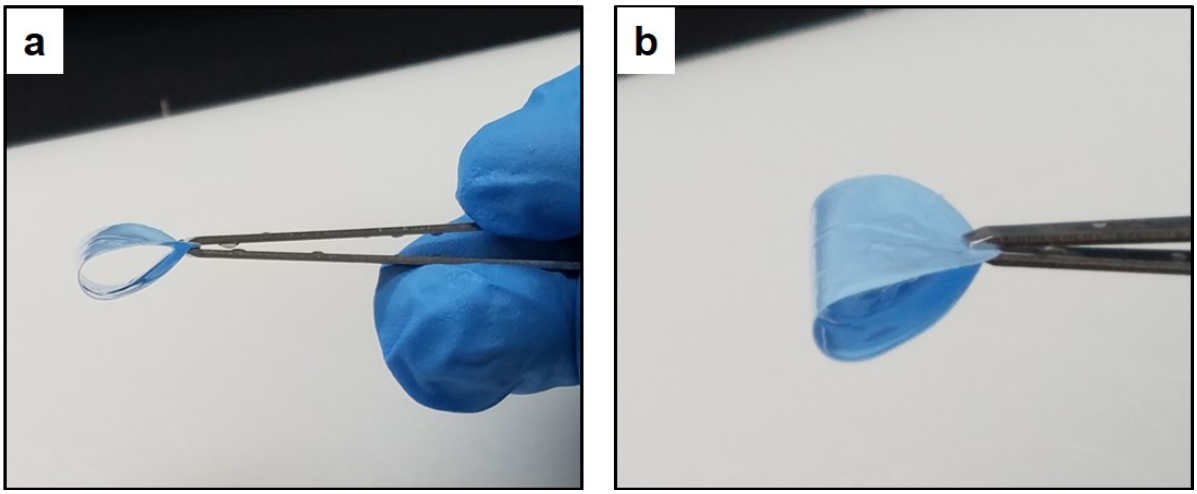

Figure S9. Photographs of the PEI-functionalized polysulfone membrane (Psf-PEI) demonstrating that the membrane is robust and easily handled. (a) Side-on view of the membrane. (b) Angled view of the membrane. The membrane was saturated with cupric chloride.

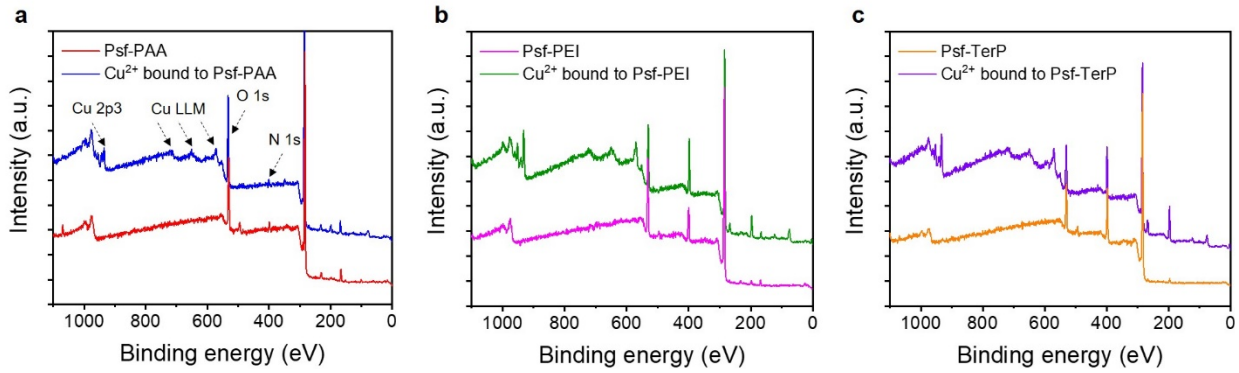

Figure S10. XPS survey spectra depicting the sequential conversion of (a) Psf-PAA to (b) Psf-PEI and to (c) Psf-TerP. The increasing ratio of the photoelectron intensity of the N 1s signal to the O 1s signal is consistent with the increasing nitrogen content that occurs due to the covalent attachment of PEI and TerP to the pore walls of the membranes. The increase of the photoelectron intensity of Cu^{2+} after the three membranes were exposed to a copper-containing solution suggests the successful adsorption of the Cu^{2+} ions to the membrane surfaces. The atomic abundance of Cu^{2+} at the surface of the membrane increased with the addition of the PEI and TerP functionality: 2.1% for the Psf-PAA material, 2.3% for the Psf-PEI membrane, and 2.6% for the Psf-TerP membrane.

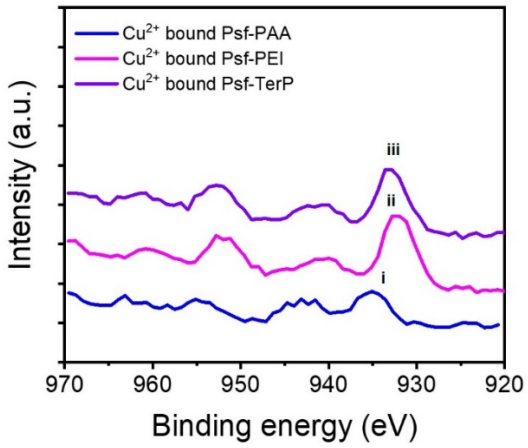

Figure S11. Magnified XPS spectra. The photoelectron intensity at 934 to 935 eV (i) for the copper ions bound to the Psf-PAA membrane is consistent with the binding energy of Cu^{2+}, 934.7 eV. The copper bound to the amine moieties of the PEI ligand (ii) and the TerP ligand (iii) partially receive donated electrons from the ligands, and hence demonstrate shifted photoelectron peaks in the range of ~932 to 933 eV.

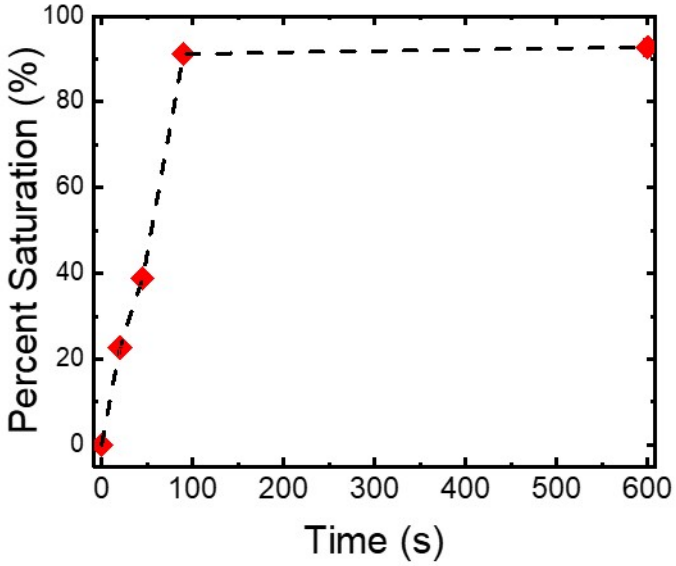

Figure S12. The adsorption kinetic experiment of the Psf-TerP membrane, in which the samples were fully immersed in a bath of excess cupric chloride solution, suggests that the ~150 µm-thick membrane achieved 90% of its equilibrium capacity within the first 90 s. To guarantee equilibrium uptake, membrane samples were left overnight (i.e., for 8 h) in solution during the binding experiments. The associated video demonstrates the color change that occurs due to Cu^{2+} uptake during exposure to a 10 mM $CuCl_2$ solution for 90 s.

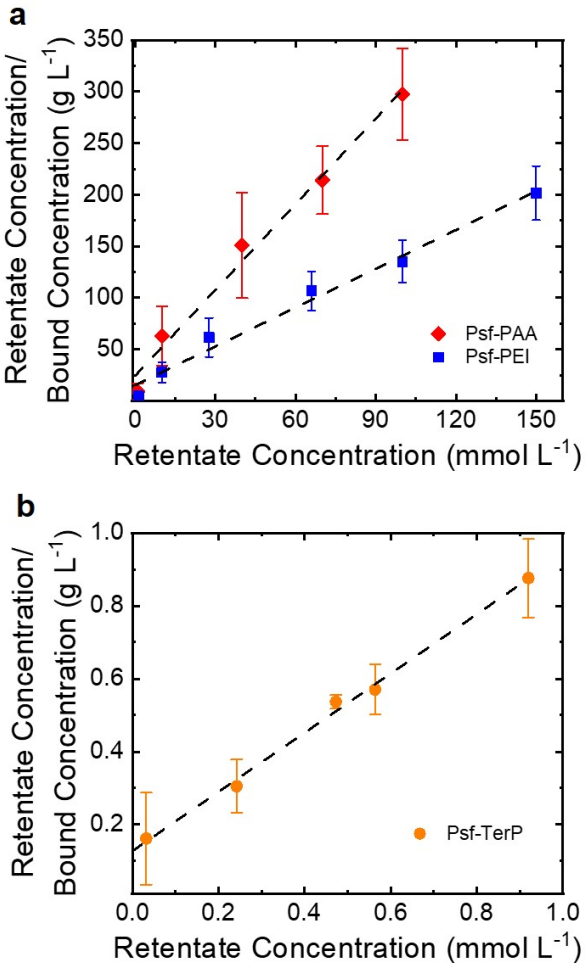

Figure S13. The linearized Langmuir isotherms of the experimental data (a) for the Psf-PAA and Psf-PEI membranes and (b) for the Psf-TerP membranes. A linear regression of these data [dashed line, where R^2 (Psf-PAA) = 98.7%, R^2 (Psf-PEI) = 98.6%, R^2 (Psf-TerP) = 99.6%] was applied in order to extract the binding affinity and saturation capacity of the three membranes for Cu^{2+}.

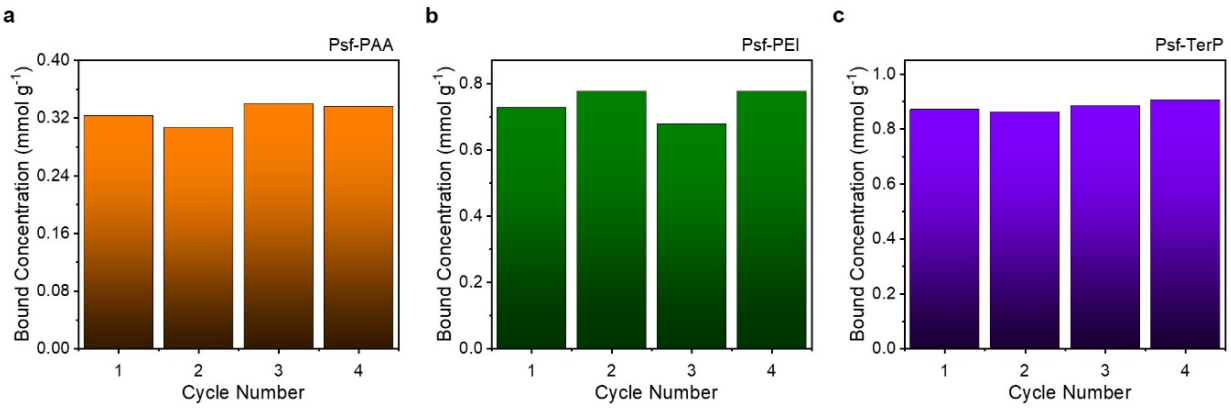

Figure S14. The equilibrium copper(II) ion uptake for the three types of Psf membranes in repeated adsorption and regeneration cycles. (a) A consistent bound ion concentration of ~0.33 mmol g^{-1} at a retentate concentration of 70 mM was observed for the Psf-PAA membrane. (b) A bound ion concentration of ~0.74 mmol g^{-1} was associated with a retentate concentration of 100 mM for the Psf-PEI membrane. (c) A bound ion concentration of ~0.88 mmol g^{-1} was retained for the Psf-TerP membrane at a retentate concentration of 0.47 mM.

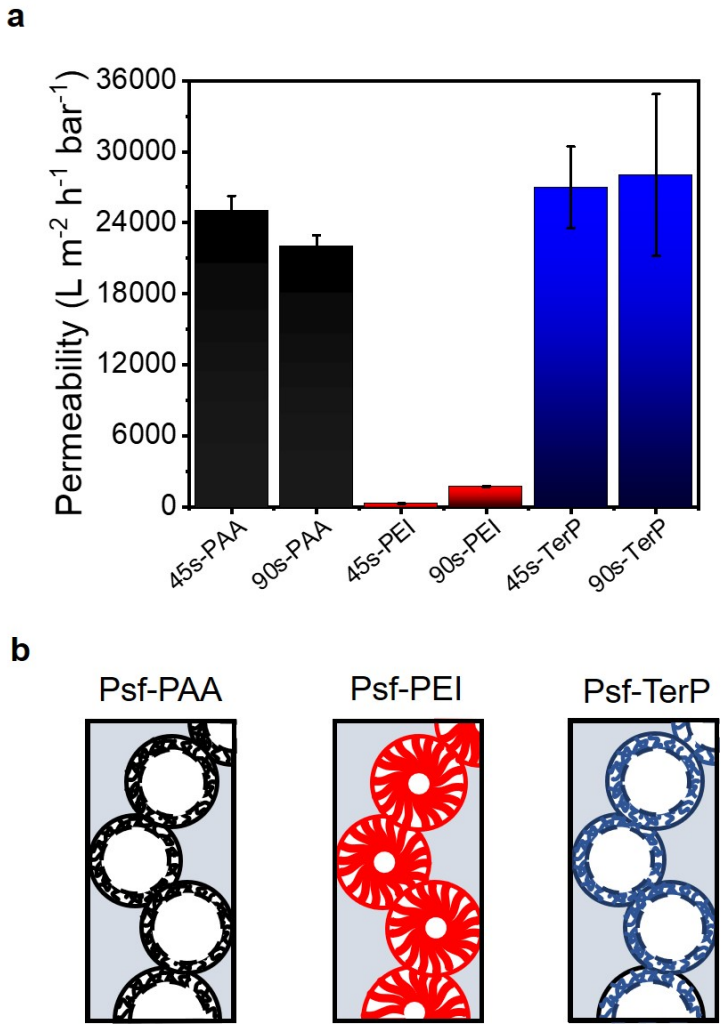

Figure S15. (a) Hydraulic permeabilities of functionalized membranes derived from the Psf-PAA-45s and Psf-PAA-90s parent membranes. Error bars are propagated standard deviation derived from multiple measurements. (b) Schematic of the hydrated polymer brush conformations, which demonstrates the effective pore size experienced during pressure-mediated flow. The attachment of the hydrophilic PEI brushes significantly reduced the pore size due to the swelling of the brushes towards the center of the pore. In turn, a lower permeability results for the Psf-PEI membrane. Furthermore, the hydrophobic nature of the TerP moieties likely cause the polymer brush to collapse back toward the pore wall, and hence produce a larger effective pore size and permeability.

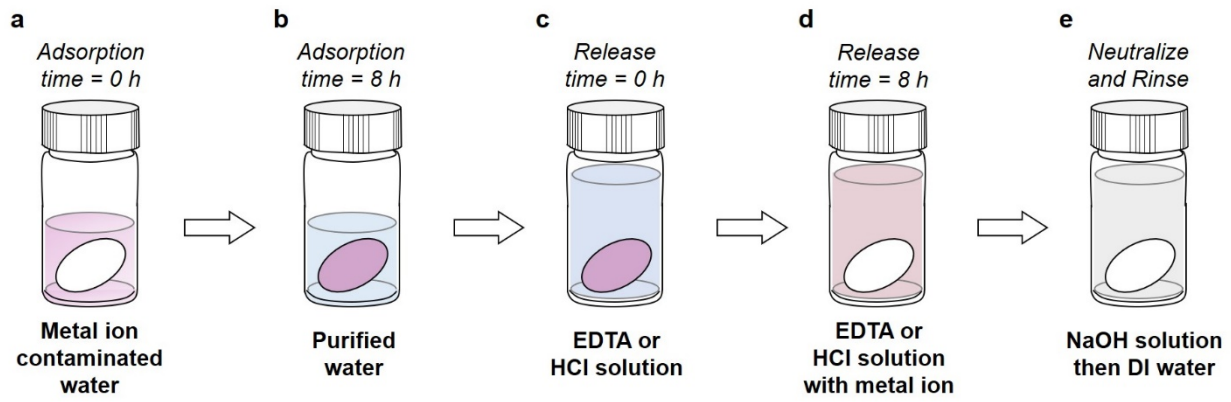

Figure S16. Schematic of the batch heavy metal uptake experiment. (a) A circular section of a membrane that was 2.5 cm in diameter was submerged in a metal-ion containing solution. (b) The membrane was submerged for 8 h. During this period, metal ions were sequestered on the sorbent surface until an apparent equilibrium was reached. (c) The metal ion-saturated membrane was then transferred to a release solution. An aqueous hydrochloric acid solution (pH 1) was used for the Psf-PAA and the Psf-PEI membranes and an aqueous 50 mM EDTA solution was used for the Psf-TerP membranes. (d) The membrane was soaked in the release solution for 8 h to ensure metal ion desorption. (e) The membranes were rinsed with excess sodium hydroxide solution (pH 13) then DI water before being recycled for subsequent adsorption experiments.

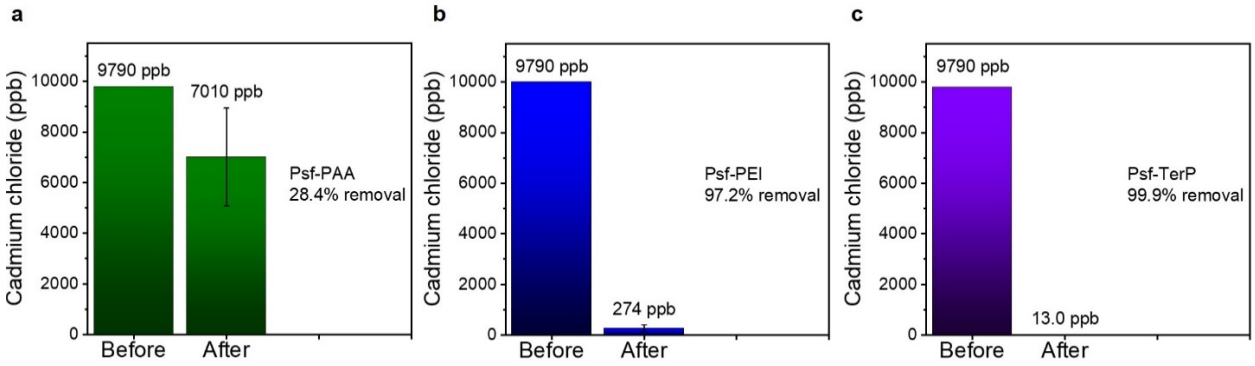

Figure S17. A set of representative data that was used to calculate the cation removal performance of (a) a Psf-PAA membrane, (b) a Psf-PEI membrane, and (c) a Psf-TerP membrane. The heavy metal ion concentrations were the measured raw data. For this experiment, an initial cadmium chloride ($CdCl_2$) concentration of 9.8 ppm (6.0 ppm Cd^{2+} ion) in artificial sea water was utilized. After the membranes were allowed to soak in solution for 8 h, the final concentrations of cadmium in solution were measured using ICP-OES. The data were then processed and reported as percentage cation removal. The Psf-TerP demonstrated the highest percent removal by producing a treated solution with a $CdCl_2$ concentration < 13 ppb (< 8.0 ppb Cd^{2+} ion).

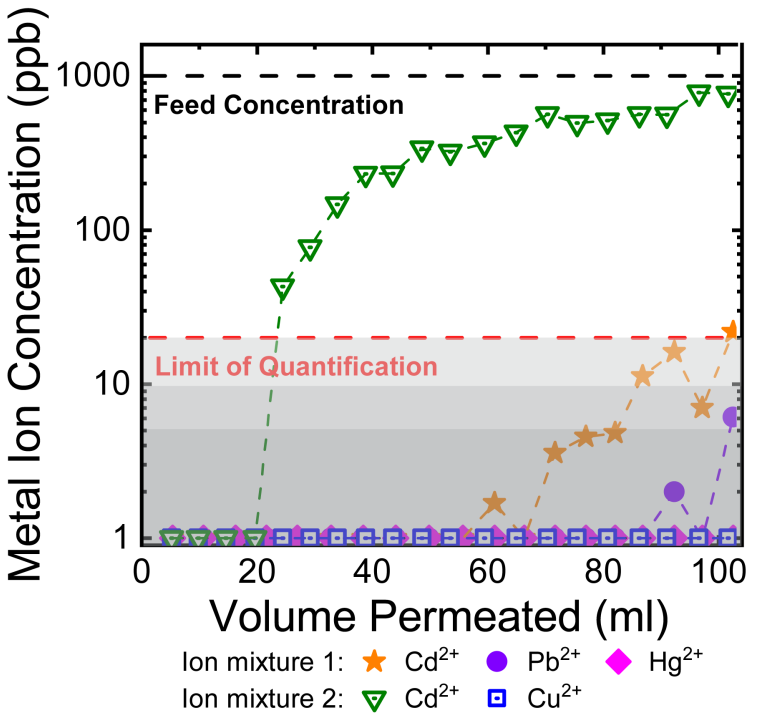

Figure S18. The ion concentration retrieved from ICP-OES analysis in the breakthrough experiment. In many instances, the concentration of heavy metal contaminants in the efflux from the membrane test bed were indistinguishable from DI water (i.e., below 1 ppb), which is below the limit of quantification (LOQ) of the ICP-OES. In the corresponding figure in the main text, the ion concentration in the permeate solution were plotted at the LOQ for the various metal ions, and this region is also shaded grey. $Cd^{2+}$and Pb^{2+} readings below their LOQ values were adjusted up to 10 ppb, while the Cu^{2+} and Hg^{2+} readings were adjusted up to 5 and 20 ppb, respectively.

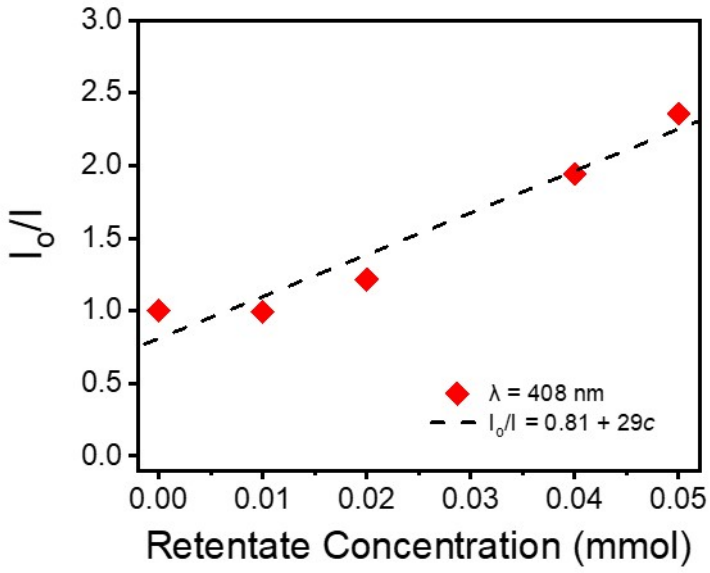

Figure S19. A Stern-Volmer plot for terpyridine fluorescence intensity as a function of the concentration of Cu^{2+} in solution. The slope of the line through the experimental data corresponds to an association constant of 2.9×10^4 L mol^{-1}.

References

1. Andres, P. R.; Lunkwitz, R.; Pabst, G. R.; Böhn, K.; Wouters, D.; Schmatloch, S.; Schubert, U. S., New 4′-functionalized 2, 2′: 6′, 2′′-terpyridines for applications in macromolecular chemistry and nanoscience. *J. Org. Chem.* **2003**, *2003*, 3769-3776.

2. Zhang, Y.; Mulvenna, R. A.; Qu, S.; Boudouris, B. W.; Phillip, W. A., Block polymer membranes functionalized with nanoconfined polyelectrolyte brushes achieve sub-nanometer selectivity. *ACS Macro Lett.* **2017**, *6*, 726-732.

3. Weidman, J. L.; Mulvenna, R. A.; Boudouris, B. W.; Phillip, W. A., Nanoporous block polymer thin films functionalized with bio-inspired ligands for the efficient capture of heavy metal ions from water. *ACS Appl. Mater. Interfaces* **2017**, *9*, 19152-19160.

4. Chave, K. E., Chemical reactions and the composition of sea water. *J. Chem. Educ*. **1971**, *48*, 148.

5. Smith, E.; Davison, W.; Hamilton-Taylor, J., Methods for preparing synthetic freshwaters. *Water Res.* **2002**, *36*, 1286-1296.

6. Schneider, C. A.; Rasband, W. S.; Eliceiri, K. W., NIH Image to ImageJ: 25 years of image analysis. *Nat. Methods* **2012**, *9*, 671-675.

7. Hiemenz, P. C.; Lodge, T. P., *Polymer Chemistry*, 2nd ed.; CRC Press: Boca Raton, FL, 2007.

8. Dukes, D.; Li, Y.; Lewis, S.; Benicewicz, B.; Schadler, L.; Kumar, S. K., Conformational transitions of spherical polymer brushes: synthesis, characterization, and theory. *Macromolecules* **2010**, *43*, 1564-1570.

9. Dimitrov, D.; Milchev, A.; Binder, K., Polymer brushes in cylindrical pores: simulation versus scaling theory. *J. Chem. Phys.* **2006**, *125*, 034905